Transition energies of the *D* lines in Na-like ions

J. D. Gillaspy,[1,*] D. Osin,[1,†] Yu. Ralchenko,[1] J. Reader,[1] and S. A. Blundell[2]
[1]*Quantum Measurement Division, National Institute of Standards and Technology, Gaithersburg, Maryland 20899-8422, USA*
[2]*SPSMS, UMR-E CEA/UJF-Grenoble 1, INAC, Grenoble, F-38054, France*
(Received 20 March 2013; published 5 June 2013)

The NIST electron beam ion trap (EBIT) was used to measure the $D_1(3s\text{-}3p_{1/2})$ and $D_2(3s\text{-}3p_{3/2})$ transitions in Na-like ions of xenon, barium, samarium, gadolinium, dysprosium, erbium, tungsten, platinum, and bismuth. The wavelengths are in the range 3–12 nm. Relativistic many-body perturbation theory calculations were carried out for the D_1 and D_2 lines for every element in the isoelectronic sequence from argon ($Z = 18$) to uranium ($Z = 92$), taking into account some higher-order terms in the quantum electrodynamics (QED) expansion. Uncertainties in the calculated values were carefully assessed by considering the uncertainties in the various contributions to the total calculated transition energies. We conclude that at the current level of accuracy, the calculated values can be taken to reliably represent the isoelectronic sequence from $Z = 18$ to 92. The agreement of theory and experiment for the D_1 line of bismuth ($Z = 83$) provides a test of QED at the level of 0.4%. Our results are also sensitive to retardation effects due to the finite speed of light and to variations in the assumed nuclear size.

DOI: 10.1103/PhysRevA.87.062503 PACS number(s): 32.30.−r, 31.15.ac, 31.30.jg, 31.30.jc

I. INTRODUCTION

Sodiumlike ions, with ground configuration $1s^2 2s^2 2p^6 3s$, have one electron outside of closed shells. They are thus similar to hydrogen, and their atomic properties can be calculated *ab initio* to high precision. By examining the uncertainties of the individual terms in the *ab initio* calculation, it is possible to reliably estimate the uncertainties of the calculated transition energies. Comparison to laboratory measurements can then be used to test the fundamental physics underlying the calculations.

Recently, Gillaspy *et al.* [1] reported new measurements of the *D* lines in several Na-like ions at high *Z*. The results were compared with multiconfiguration Dirac-Fock (MCDF) calculations of Kim *et al.* [2]. Although the overall agreement was generally good, for the $D_1(3s\text{-}3p_{1/2})$ lines the calculations of Kim *et al.* [2] produced wavelengths that were up to 0.003 nm shorter than were observed at high *Z* (where the wavelengths are approximately 8 nm). The wavelengths of Kim *et al.* [2] were also systematically shorter, by about the same amount, than those given in the subsequent many-body perturbation theory (MBPT) calculations of Blundell [3]. For the $D_2(3s\text{-}3p_{3/2})$ lines, some puzzling differences between the experimental and calculated values could be seen in the region $Z = 50$–65. Gillaspy *et al.* [1] concluded by calling for new measurements in this region and for new high-accuracy calculations for $Z > 65$, where the paucity of theoretical results made a comparison of theory with experiment difficult. In the present paper we address both of these needs. We made measurements for Xe ($Z = 54$), Ba ($Z = 56$), Sm ($Z = 62$), Gd ($Z = 64$), Dy ($Z = 66$), Er ($Z = 68$), W ($Z = 74$), Pt ($Z = 78$), and Bi ($Z = 83$), and performed MBPT calculations for all Na-like ions in the range $Z = 18$–92.

II. EXPERIMENT

Highly charged ions were produced, trapped, and excited with the electron beam ion trap (EBIT) at the National Institute of Standards and Technology (NIST) [4]. Spectra were recorded with an extreme ultraviolet (EUV) spectrometer designed especially for use with our EBIT [5]. Subsequent to an earlier experiment on magnetic dipole transitions in highly charged tungsten [6], the detector on the spectrometer was replaced with one having more pixels of smaller size (13.5 μm × 13.5 μm) and lower noise. This provided improved performance for our observations.

Spectra were recorded in three separate runs over the course of several months. For each run, calibrations were performed daily, typically before and after collecting data for the element under investigation. Wavelength calibration was provided by spectra of C, N, O, Ne, Ar, and Fe. These were all observed separately, except for C and O, which were measured together using injected CO_2 gas. Depending on the element, the trap was loaded from the side, top, or bottom, using one of the following three methods.

(a) Gases were continuously loaded from the side as neutral atoms (across the magnetic field lines) using the system described by Fahy *et al.* [7], with a typical injection pressure $P1 = 1 \times 10^{-4}$ hPa (7.5×10^{-5} Torr).

(b) Metal elements were loaded as ions along the magnetic field axis using a multicathode metal vapor vacuum arc (MEVVA) ion source [8] located 2 m above the center of the EBIT and held at the 10 keV loading potential of the EBIT drift tubes. The ions were captured in the trap by lowering the potential of the middle drift tube as the ions decelerated into the trap center. After loading, the voltage of the entire drift tube assembly was changed to the nominal value used for the particular measurement (specified below). To minimize the buildup of contaminants, the trap was emptied and reloaded every 10 s. During loading, the voltage in the drift tubes deviated from the nominal value for <0.01 s per cycle. Photons were collected continuously.

*john.gillaspy@nist.gov
†Present address: Tri Alpha Energy Inc., Rancho Santa Margarita, CA 92688, USA.

(c) Ba was loaded from below by stopping the procedure for periodically emptying the trap described above. This allowed the trap to load continuously with Ba from the electron gun, as described previously [9]. Additionally, we reversed the asymmetry of the end drift tube potentials so they would have the proper orientation for loading ions from the bottom of the EBIT, where the electron gun is located. The drift tube farthest from the Ba source was biased 500 V above the center drift tube, while the drift tube closest to the Ba source was biased at 220 V. This reverse bias increased the Ba signal when the drift tube potential was lower than the potential of the transition electrode described in Ref. [4]. This suggested that a significant amount of Ba was ionized in transit to the trap.

Spectra were recorded at nominal electron beam energies (not corrected for space-charge effects) as follows: 8490, 9000, 10 000, 13 000, 20 000, and 30 000 eV (Ba), 30 040 eV (Xe), 10 000 eV (Sm), 10 840 eV (Gd, Dy, Er), 15 090 eV (W), 23 970 eV (Pt), and 28 570 and 30 040 eV (Bi).

III. WAVELENGTH DETERMINATIONS

The spectra were calibrated by using several dozen lines with well-known wavelengths from the calibration elements, distributed across our region of observation. Wavelengths were taken from the NIST Atomic Spectra Database [10], with uncertainties taken from the original literature. Wavelengths were determined by a fourth-order polynomial describing wavelength versus position on the detector. The calibration lines were weighted according to the quadrature sum of three components: the assigned uncertainty of the wavelength (typically 0.0005 nm or less), the statistical uncertainty of the measured position of the calibration line in our spectrum (<0.0002 nm for strong lines), and an additional systematic measurement uncertainty corresponding to approximately 0.1 pixel (0.0005–0.0011 nm) determined by requiring that the reduced chi square of the fit to be equal to 1.0. The residuals of the fit were symmetric and without baseline offset or bias in the mean, so their standard deviation was taken to represent the overall uncertainty of the calibration. The total uncertainties in the wavelengths are taken to be the quadrature sum of the calibration uncertainty, the statistical uncertainty in the observed position of a particular line, and the additional systematic measurement uncertainty (corresponding to approximately 0.1 pixel) mentioned above. When new lines were observed in both first and second order of diffraction, the wavelengths and uncertainties obtained in second order were divided by two and the weighted average was taken together with their first-order results. Calibration lines were used only in first order.

Lines were fit to a Gaussian profile over a range which extended from the peak intensity to approximately 10% of the peak intensity. In order to reduce the possibility of errors from coincidental line blends or imperfect removal of cosmic ray events, fits were scrutinized for anomalous width or shape, and examined for dependence of intensity and/or centroid on electron beam energy when the data allowed.

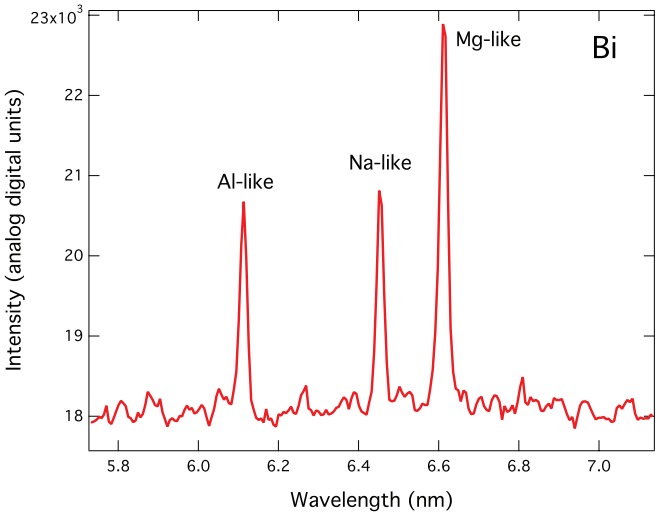

FIG. 1. (Color online) Bi spectrum near the D_1 line. Also shown are the neighboring $2p_{1/2}$-$3d_{3/2}$ line in Al-like Bi and the $3s^2(1/2,1/2)_0$-$3s3p(1/2,3/2)_1$ line in Mg-like Bi.

IV. EXPERIMENTAL RESULTS

Figure 1 shows a section of our spectrum for Bi. This represents the sum of several spectra of duration 20 min or less, for a total acquisition time of 2.5 h. Collisional-radiative modeling [6] was used to aid in the line identification. Table I contains the results of the present measurements. Here, and throughout this paper, error estimates are presented at the one standard uncertainty level. Wavelengths for Xe were previously measured by Seely *et al*. using the PLT tokamak: 12.392(3) and 6.658(3) nm. These were unpublished values quoted in the paper by Seely and Wagner [11]. Trabert *et al*. [12] gave the value 6.6574(20) nm as measured in the EBIT at the Lawrence Livermore National Laboratory, and Fahy *et al*. [7] reported the value 6.657(3) nm from an earlier experiment on the NIST EBIT. Because it has been reported previously [13] that the measured wavelength of the D_2 line in xenon appeared to have an energy dependence that might indicate the presence of an unresolved blend, we note that our present measurement for xenon was done at approximately 30 keV, a substantially higher beam energy than used previously. This should reduce the chance of blends with lines of lower charge states, and indeed our result is substantially different

TABLE I. Measured wavelengths (nm) for D lines of several Na-like ions.

	Z	Stage	$D_1(3s_{1/2}$-$3p_{1/2})$	Unc.	$D_2(3s_{1/2}$-$3p_{3/2})$	Unc.
Xe	54	43+	12.394	0.001	6.6628	0.0005
Ba	56	45+	11.767	0.001	5.9848	0.0005
Sm	62	51+	10.154	0.001	4.349	0.001
Gd	64	53+	9.690	0.001	3.912	0.001
Dy	66	55+	9.257	0.001	3.520	0.001
Er	68	57+	8.850	0.001	3.171	0.001
W	74	63+	7.7697	0.0011		
Pt	78	67+	7.1451	0.0011		
Bi	83	72+	6.4547	0.0005		

from those of the previous measurements. For W, our present value of 7.7697(11) nm for D_1 agrees well with our earlier measurement of 7.7700(12) nm [1]. For Gd, our value of 3.912(1) nm for D_2 is somewhat high compared to the earlier measurement of Seely *et al*. [14] of 3.9075(20) nm.

V. THEORY

Tables II(a) and II(b) list the wave numbers ($\sigma = E/hc$) and wavelengths ($\lambda = hc/E$) obtained from the calculated transition energies, along with their associated uncertainties (Unc.), for all elements in the range $Z = 18$–92. These results were obtained following the earlier work already mentioned [3]. Our present calculations used larger basis sets and higher numerical accuracy. Results were also obtained for elements that were not tabulated in Ref. [3]. A few extra small terms were also added to the calculation, and a careful treatment of the error arising from uncertainty in the root-mean-square (rms) radius of the nucleus was made.

The various terms that contribute to the total transition energy are listed for the case of Bi in Table III. The first row in the table gives the Coulomb Dirac-Hartree-Fock (DHF) energy, while the other rows contain the additional contributions described below.

Overall, the theoretical treatment considers (in some approximation) all second-order effects in quantum electrodynamics (QED) perturbation theory beyond the zeroth-order DHF treatment, that is, incorporating effects described by Feynman diagrams with up to two exchanged photons. We also add one third-order (three-photon) effect associated with relativistic correlation. Two small two-photon terms (denoted "other retardation" and "other vertex" in Table III) were taken to be zero rather than evaluated explicitly, but uncertainty estimates for this approximation were included. The Appendix describes more completely all of the terms included. The leading terms not considered should be smaller than the highest order terms considered by factors of $1/Z_s$, α/π, or $(Z_s\alpha)^2$, where $Z_s = Z - 10$ is the effective (screened) nuclear charge.

The theoretical uncertainties in Table III are determined as follows. The uncertainty for the DHF value reflects the uncertainty in the rms nuclear radius, as described below. The uncertainties on "other retardation" and "other vertex" terms are estimates of the likely size of these terms (see the Appendix), which were not calculated. The uncertainty for the two-loop Lamb shift includes the uncertainty from Ref. [15] on the $1s$ hydrogenic value, combined with an additional estimated uncertainty for our scaling procedure to convert this value to the transitions in Na-like ions. The error on nuclear recoil is taken as $(Z\alpha)^2$ times the term tabulated to account for omitted higher-order relativistic effects. All the other uncertainties are estimates of our numerical uncertainty in evaluating well-defined perturbation-theory terms. The final theory uncertainty is estimated by adding the individual uncertainties in quadrature.

In addition to the self-energy (SE) and vacuum-polarization (VP) contributions to the QED shifts, we now include an estimate for the two-loop Lamb shift. The total vacuum polarization includes both Uehling and Wichmann-Kroll (WK) terms. The following contributions to the self-energy and vacuum polarization terms are listed separately in Table III: (1) valence QED contributions screened by the direct (classical electrostatic) interaction with the core electrons (denoted "val"), (2) the valence-exchange correction (denoted "val-exch"), in which the valence SE or VP is modified by the exchange (as opposed to direct) interaction with the core (the DHF potential of the core is a sum of direct and exchange terms, the latter arising from the Fermi statistics of indistinguishable electrons), and (3) core-relaxation terms (denoted "core-rlx"), corresponding to the change in SE or VP of the core as the valence electron changes in the transition. Contributions (2) and (3) are relatively small but nevertheless essential at the present level of accuracy. In evaluating (2) and (3), we assumed that the associated vertex corrections were numerically small and set them equal to zero ("other vertex"); an uncertainty estimate was added to these terms to account for their likely size.

We refer to the sum of the 12th through 20th terms (rows in Table III, between the dotted lines) as the QED contribution (given in Table II), and the rest of the terms as the relativistic many-body perturbation theory (RMBPT) contribution. This terminology follows historical usage (e.g., Ref. [16]), but it should be noted that both types of terms contain relativistic and field-theoretic effects. The three Coulomb-photon exchange term, here denoted CCC(3) but previously called E(3) [16], appears small as a result of the near perfect cancellation of two larger numbers (from the difference between levels). In fact, CCC(3) passes through zero near $Z = 23$. To check for possible errors due to the near perfect cancellation, the difference $3p - 3s$ was formed and tested for stability by varying all of the relevant numerical parameters in the calculation (number of basis functions, radial grid size, etc.).

The nuclear radii (together with their uncertainties) given in the second and third to the last columns in Table II are taken from Ref. [17], except for Th and U, where the values are taken from Refs. [18] and [19], and Xe, Yb, and Hg, where the values are taken from Ref. [15] (which itself is based on Refs. [20,21]). We assume a Fermi distribution of nuclear charge, with a skin thickness (over which the density drops from 90% to 10% of its maximum value) of 2.3 fm. The uncertainty quoted for the DHF value corresponds to the change in the DHF value when the rms nuclear radius is increased by one standard deviation. We have increased this change by an additional 10% to allow for possible model dependence arising from the use of a Fermi distribution. Other terms in the calculation include significant finite nuclear-size contributions, notably the self-energy and Uehling QED terms, but the dominant nuclear-finite-size effect arises from the DHF term, and we restrict the uncertainty to this term.

The last column of Tables II(a) and II(b) gives the sensitivity of the transition energy to small changes in the nuclear radius about the assumed values (the negative sign means that an increase in radius results in a reduction in transition energy). One use of this column is to correct the theoretical transition energy for a different assumed nuclear radius. As an example, consider the D_1 transition energy for Bi, where we assumed an rms nuclear radius of 5.531(5) fm, and the sensitivity coefficient is -6804 cm^{-1} fm^{-1}. For an rms radius of 5.548(25) fm, the transition energy should be corrected by $-6804 \times (5.548 - 5.531) = -116$ cm^{-1}.

TABLE II. Theoretical and experimental data for the (a) $D_1(3s_{1/2}\text{-}3p_{1/2})$ and (b) $D_2(3s_{1/2}\text{-}3p_{3/2})$ lines of sodium-like ions from Ar^{7+} to U^{81+}.

(a)			Theory					Experiment					$\Delta\sigma$	Nuc.		Nucl.
	Z	Stage	σ (cm^{-1})	Unc. (cm^{-1})	λ (nm)	Unc. (nm)	QED (cm^{-1})	σ (cm^{-1})	Unc. (cm^{-1})	λ (nm)	Unc. (nm)	Reference	(th-expt.) (cm^{-1})	size (fm)	Unc. (fm)	coeff. (cm^{-1}/fm)
Ar	18	7+	140095.0	2.7	71.3801	0.0014	−132.6	140093.3	5.9	71.381	0.003	[23]	1.7	3.428	0.008	−0.576
K	19	8+	157157.8	3.2	63.6303	0.0013	−173.4	157152.4	2.5	63.6325	0.0010	[23]	5.4	3.407	0.025	−0.755
Ca	20	9+	174217.1	4.1	57.3997	0.0014	−221.9	174213.0	3.0	57.4010	0.0010	[23]	4.1	3.476	0.007	−1.00
Sc	21	10+	191290.0	4.7	52.2766	0.0013	−277.0	191288.0	3.7	52.2772	0.0010	[23]	2.0	3.542	0.050	−1.37
Ti	22	11+	208387.2	5.2	47.9876	0.0012	−340.8	208385.0	4.3	47.9881	0.0010	[23]	2.2	3.599	0.009	−1.78
V	23	12+	225519.3	5.5	44.3421	0.0011	−413.6	225518.8	5.1	44.3422	0.0010	[23]	0.5	3.602	0.025	−2.26
Cr	24	13+	242695.6	5.9	41.2039	0.0010	−495.3	242688.4	2.4	41.2051	0.0004	[23]	7.2	3.612	0.061	−2.87
Mn	25	14+	259920.4	6.2	38.4733	0.0009	−589.7	259915.8	33.8	38.474	0.005	[23]	4.7	3.705	0.055	−3.65
Fe	26	15+	277204.4	6.6	36.0745	0.0009	−694.6	277191.8	3.1	36.0761	0.0004	[23]	12.6	3.736	0.003	−4.46
Co	27	16+	294551.5	7.1	33.9499	0.0008	−812.5	294542.1	17.4	33.951	0.0020	[23]	9.4	3.782	0.034	−5.56
Ni	28	17+	311966.7	7.5	32.0547	0.0008	−945.9	311949.2	5.8	32.0565	0.0006	[23]	17.5	3.776	0.020	−6.72
Cu	29	18+	329457.9	7.9	30.3529	0.0007	−1092.6	329441.5	10.9	30.3544	0.0010	[23]	16.4	3.898	0.007	−8.34
Zn	30	19+	347028.7	8.6	28.8161	0.0007	−1256.1	347007.8	12.0	28.8178	0.0010	[23]	21.0	3.955	0.047	−10.1
Ga	31	20+	364684.8	9.3	27.4209	0.0007	−1436.8	364681.3	13.3	27.4212	0.0010	[23]	3.5	3.998	0.050	−12.2
Ge	32	21+	382431.0	10.2	26.1485	0.0007	−1635.4	382409.2	14.6	26.1500	0.0010	[23]	21.8	4.079	0.050	−14.6
As	33	22+	400276.4	10.8	24.9827	0.0007	−1850.2	400253.0	16.0	24.9842	0.0010	[23]	23.4	4.104	0.002	−17.1
Se	34	23+	418221.3	11.8	23.9108	0.0007	−2085.4	418194.8	17.5	23.9123	0.0010	[23]	26.5	4.171	0.050	−20.6
Br	35	24+	436275.4	12.7	22.9213	0.0007	−2339.9	436256.4	19.0	22.9223	0.0010	[23]	19.0	4.156	0.050	−23.9
Kr	36	25+	454438.7	13.8	22.0052	0.0007	−2615.9	454427.7	20.7	22.0057	0.0010	[23]	11.0	4.230	0.050	−28.3
Rb	37	26+	472720.7	14.9	21.1541	0.0007	−2913.9							4.245	0.050	−32.9
Sr	38	27+	491127.2	16.0	20.3613	0.0007	−3233.4							4.242	0.036	−37.9
Y	39	28+	509660.6	17.4	19.6209	0.0007	−3577.1	509645.0	26.0	19.6215	0.0010	[23]	15.6	4.244	0.002	−43.3
Zr	40	29+	528328.5	18.5	18.9276	0.0007	−3943.3	528326.2	27.9	18.9277	0.0010	[23]	2.3	4.273	0.001	−50.3
Nb	41	30+	547130.1	20.0	18.2772	0.0007	−4339.3	547114.8	29.9	18.2777	0.0010	[23]	15.3	4.318	0.003	−57.9
Mo	42	31+	566074.5	21.5	17.6655	0.0007	−4759.2	566039.9	32.0	17.6666	0.0010	[23]	34.6	4.415	0.006	−67.6
Tc	43	32+	585175.0	23.4	17.0889	0.0007	−5205.5							4.410	0.050	−77.2
Ru	44	33+	604428.3	25.0	16.5446	0.0007	−5679.0							4.475	0.050	−89.0
Rh	45	34+	623845.7	26.4	16.0296	0.0007	−6181.0							4.502	0.030	−101
Pd	46	35+	643431.1	28.7	15.5417	0.0007	−6712.7							4.526	0.050	−115
Ag	47	36+	663191.0	29.8	15.0786	0.0007	−7276.1	663217.9	219.9	15.078	0.005	[23]	−26.9	4.542	0.002	−130
Cd	48	37+	683120.9	31.8	14.6387	0.0007	−7870.2	683027.5	70.0	14.6407	0.0015	[14]	93.5	4.613	0.002	−149
In	49	38+	703249.1	33.9	14.2197	0.0007	−8498.6							4.619	0.015	−168
Sn	50	39+	723561.9	35.8	13.8205	0.0007	−9162.0	723856.1	78.6	13.8149	0.0015	[14]	−294.2	4.655	0.001	−191
Sb	51	40+	744070.7	39.9	13.4396	0.0007	−9860.3							4.704	0.050	−217
Te	52	41+	764768.9	42.5	13.0758	0.0007	−10597.2							4.804	0.050	−248
I	53	42+	785717.0	42.8	12.7272	0.0007	−11371.7							4.752	0.011	−274
Xe	54	43+	806857.6	48.4	12.3938	0.0007	−12186.3	806842.0	65.1	12.394	0.001	This work	15.6	4.787	0.051	−310
Cs	55	44+	828233.9	47.8	12.0739	0.0007	−13041.1							4.807	0.001	−347
Ba	56	45+	849833.5	50.6	11.7670	0.0007	−13938.6	849834.3	72.2	11.767	0.001	This work	−0.8	4.840	0.001	−389
La	57	46+	871678.7	53.4	11.4721	0.0007	−14878.9							4.855	0.001	−436
Ce	58	47+	893768.8	56.4	11.1886	0.0007	−15864.8							4.877	0.001	−487
Pr	59	48+	916121.9	59.5	10.9156	0.0007	−16894.7							4.893	0.001	−545
Nd	60	49+	938728.8	62.7	10.6527	0.0007	−17973.6							4.915	0.001	−609
Pm	61	50+	961594.5	76.0	10.3994	0.0008	−19100.2							4.962	0.050	−685
Sm	62	51+	984707.9	87.6	10.1553	0.0009	−20277.6	984833.6	97.0	10.154	0.0010	This work	−125.6	5.031	0.063	−770
Eu	63	52+	1008155.2	86.9	9.9191	0.0009	−21505.5							5.041	0.050	−856
Gd	64	53+	1031870.5	93.2	9.6911	0.0009	−22786.9	1031991.7	106.5	9.690	0.0010	This work	−121.3	5.089	0.050	−957
Tb	65	54+	1055917.4	99.7	9.4704	0.0009	−24121.4							5.099	0.050	−1064
Dy	66	55+	1080307.2	135.0	9.2566	0.0012	−25511.4	1080263.6	116.7	9.257	0.0010	This work	43.6	5.083	0.081	−1180
Ho	67	56+	1104844.7	137.0	9.0510	0.0011	−26957.4							5.210	0.071	−1330
Er	68	57+	1129988.8	151.0	8.8496	0.0012	−28463.0	1129943.5	127.7	8.850	0.0010	This work	45.2	5.123	0.074	−1456
Tm	69	58+	1155245.8	133.0	8.6562	0.0010	−30027.1							5.192	0.050	−1625
Yb	70	59+	1180735.3	145.0	8.4693	0.0010	−31651.1							5.317	0.051	−1829
Lu	71	60+	1206917.8	154.0	8.2856	0.0011	−33341.1							5.246	0.050	−2005

TABLE II. (*Continued*.)

(a)			Theory					Experiment					$\Delta\sigma$	Nuc.		Nucl.
	Z	Stage	σ (cm^{-1})	Unc. (cm^{-1})	λ (nm)	Unc. (nm)	QED (cm^{-1})	σ (cm^{-1})	Unc. (cm^{-1})	λ (nm)	Unc. (nm)	Reference	(th-expt.) (cm^{-1})	size (fm)	Unc. (fm)	coeff. (cm^{-1}/fm)
Hf	72	61+	1233268.2	167.0	8.1085	0.0011	−35094.3	1233319.4	182.5	8.1082	0.0012	[1]	−51.2	5.290	0.050	−2230
Ta	73	62+	1260051.7	180.0	7.9362	0.0011	−36913.7	1259794.9	190.4	7.9378	0.0012	[1]	256.8	5.299	0.050	−2468
W	74	63+	1287068.5	223.0	7.7696	0.0013	−38800.2	1287051.0	182.2	7.7697	0.0011	This work	17.5	5.359	0.061	−2750
Re	75	64+	1314672.2	214.0	7.6065	0.0012	−40756.7							5.351	0.050	−3034
Os	76	65+	1342562.4	230.0	7.4484	0.0013	−42781.1							5.376	0.050	−3361
Ir	77	66+	1370845.3	250.0	7.2948	0.0013	−44880.6							5.401	0.050	−3723
Pt	78	67+	1399575.7	275.0	7.1450	0.0014	−47051.3	1399560.5	215.5	7.1451	0.0011	This work	15.1	5.418	0.050	−4118
Au	79	68+	1428702.9	175.0	6.9994	0.0009	−49297.7	1428755.1	245.0	6.9991	0.0012	[1]	−52.2	5.437	0.011	−4546
Hg	80	69+	1458176.3	170.0	6.8579	0.0008	−51624.8							5.467	0.006	−5053
Tl	81	70+	1488149.2	175.0	6.7198	0.0008	−54027.5							5.483	0.001	−5562
Pb	82	71+	1518511.8	186.0	6.5854	0.0008	−56506.8							5.505	0.001	−6150
Bi	83	72+	1549260.6	199.0	6.4547	0.0008	−59072.0	1549258.7	120.0	6.4547	0.0005	This work	1.9	5.531	0.005	−6804
Po	84	73+	1580557.1	464.0	6.3269	0.0019	−61721.3							5.539	0.050	−7528
At	85	74+	1612033.3	508.0	6.2033	0.0020	−64450.3							5.578	0.050	−8333
Rn	86	75+	1643736.1	557.0	6.0837	0.0021	−67270.1							5.632	0.050	−9234
Fr	87	76+	1676270.3	614.0	5.9656	0.0022	−70175.6							5.640	0.050	−10189
Ra	88	77+	1709055.3	685.0	5.8512	0.0023	−73170.8							5.663	0.050	−11255
Ac	89	78+	1742362.1	739.0	5.7393	0.0024	−76248.9							5.670	0.050	−12415
Th	90	79+	1774385.8	324.0	5.6358	0.0010	−79418.6							5.802	0.004	−13805
Pa	91	80+	1809911.5	893.0	5.5251	0.0027	−82690.5							5.700	0.050	−15122
U	92	81+	1841739.8	332.0	5.4296	0.0010	−86037.2							5.860	0.002	−16840
(b)																
Ar	18	7+	142804.6	3.0	70.02574	0.00146	−126.0	142808.2	6.1	70.024	0.003	[23]	−3.6	3.428	0.008	−0.576
K	19	8+	160916.1	2.9	62.14420	0.00110	−164.2	160913.5	2.6	62.1452	0.0010	[23]	2.6	3.407	0.025	−0.755
Ca	20	9+	179288.1	3.6	55.77613	0.00111	−209.6	179287.6	3.2	55.7763	0.0010	[23]	0.5	3.476	0.007	−1.00
Sc	21	10+	197978.1	4.2	50.51065	0.00107	−260.9	197981.0	3.9	50.5099	0.0010	[23]	−2.9	3.542	0.050	−1.37
Ti	22	11+	217039.2	4.6	46.07463	0.00098	−320.3	217041.7	4.7	46.0741	0.0010	[23]	−2.5	3.599	0.009	−1.76
V	23	12+	236528.8	5.0	42.27815	0.00090	−387.5	236525.2	5.6	42.2788	0.0010	[23]	3.6	3.602	0.025	−2.26
Cr	24	13+	256504.4	5.4	38.98568	0.00081	−463.3	256499.7	2.0	38.9864	0.0003	[23]	4.7	3.612	0.061	−2.87
Mn	25	14+	277023.9	5.8	36.09797	0.00075	−549.9	277026.0	7.7	36.0977	0.0010	[23]	−2.1	3.705	0.055	−3.66
Fe	26	15+	298152.0	6.1	33.53994	0.00069	−646.4	298142.6	2.7	33.5410	0.0003	[23]	9.4	3.736	0.003	−4.54
Co	27	16+	319951.9	6.7	31.25469	0.00065	−754.6	319948.8	20.5	31.255	0.002	[23]	3.1	3.782	0.034	−5.58
Ni	28	17+	342491.0	7.2	29.19785	0.00061	−876.8	342477.5	23.5	29.199	0.002	[23]	13.5	3.776	0.020	−6.75
Cu	29	18+	365841.4	7.7	27.33425	0.00057	−1011.1	365828.7	13.4	27.3352	0.0010	[23]	12.7	3.898	0.007	−8.37
Zn	30	19+	390076.4	8.3	25.63600	0.00055	−1160.4	390061.2	15.2	25.6370	0.0010	[23]	15.2	3.955	0.047	−10.2
Ga	31	20+	415273.4	9.0	24.08052	0.00052	−1325.7	415265.1	17.2	24.0810	0.0010	[23]	8.3	3.998	0.050	−12.2
Ge	32	21+	441514.3	9.9	22.64932	0.00051	−1506.2	441507.0	19.5	22.6497	0.0010	[23]	7.4	4.079	0.050	−14.7
As	33	22+	468886.3	10.6	21.32713	0.00048	−1701.8	468878.2	22.0	21.3275	0.0010	[23]	8.1	4.104	0.002	−17.3
Se	34	23+	497474.3	11.5	20.10154	0.00046	−1915.5	497487.7	24.7	20.1010	0.0010	[23]	−13.3	4.171	0.050	−20.8
Br	35	24+	527375.4	12.5	18.96182	0.00045	−2146.2	527365.0	27.8	18.9622	0.0010	[23]	10.5	4.156	0.050	−24.2
Kr	36	25+	558680.7	13.6	17.89931	0.00044	−2396.2	558690.4	31.2	17.8990	0.0010	[23]	−9.8	4.230	0.050	−28.5
Rb	37	26+	591495.2	14.8	16.90631	0.00042	−2665.7							4.245	0.050	−33.2
Sr	38	27+	625925.8	16.1	15.97634	0.00041	−2953.1	625899.7	19.6	15.9770	0.0005	[23]	26.0	4.242	0.036	−38.3
Y	39	28+	662075.5	17.4	15.10402	0.00040	−3264.5	662098.2	43.8	15.1035	0.0010	[23]	−22.7	4.244	0.002	−43.9
Zr	40	29+	700063.9	18.7	14.28441	0.00038	−3594.4	700088.9	49.0	14.2839	0.0010	[23]	−25.0	4.273	0.001	−50.9
Nb	41	30+	740002.5	20.2	13.51347	0.00037	−3951.3	739984.3	54.8	13.5138	0.0010	[23]	18.2	4.318	0.003	−58.7
Mo	42	31+	782018.0	21.8	12.78743	0.00036	−4329.4	782025.9	61.2	12.7873	0.0010	[23]	−7.9	4.415	0.006	−68.5
Tc	43	32+	826248.2	23.9	12.10290	0.00035	−4730.3							4.410	0.050	−78.4
Ru	44	33+	872816.6	25.7	11.45716	0.00034	−5155.5	872935.5	114.3	11.4556	0.0015	[23]	−118.9	4.475	0.050	−90.4
Rh	45	34+	921868.4	27.3	10.84754	0.00032	−5605.8	921879.9	127.5	10.8474	0.0015	[23]	−11.5	4.502	0.030	−103
Pd	46	35+	973546.4	29.8	10.27172	0.00031	−6082.4	973605.6	142.2	10.2711	0.0015	[23]	−59.2	4.526	0.050	−118
Ag	47	36+	1028001.8	31.1	9.72761	0.00029	−6587.2	1028140.2	158.6	9.7263	0.0015	[23]	−138.4	4.542	0.002	−133
Cd	48	37+	1085380.1	33.4	9.21336	0.00028	−7119.7	1085564.2	176.8	9.2118	0.0015	[14]	−184.0	4.613	0.002	−152

TABLE II. (*Continued*.)

(b)			Theory					Experiment					$\Delta\sigma$	Nuc.		Nucl.
	Z	Stage	σ (cm^{-1})	Unc. (cm^{-1})	λ (nm)	Unc. (nm)	QED (cm^{-1})	σ (cm^{-1})	Unc. (cm^{-1})	λ (nm)	Unc. (nm)	Reference	(th-expt.) (cm^{-1})	size (fm)	Unc. (fm)	coeff. (cm^{-1}/fm)
In	49	38+	1145868.2	35.9	8.72701	0.00027	−7680.2	1145974.2	197.0	8.7262	0.0015	[14]	−106.0	4.619	0.015	−172
Sn	50	39+	1209609.5	38.1	8.26713	0.00026	−8276.2	1209731.1	219.5	8.2663	0.0015	[14]	−121.6	4.655	0.001	−195
Sb	51	40+	1276790.2	42.5	7.83214	0.00026	−8901.3	1276959.8	326.1	7.8311	0.0020	[24]	−169.6	4.704	0.050	−222
Te	52	41+	1347577.2	45.6	7.42073	0.00025	−9561.5							4.804	0.050	−254
I	53	42+	1422216.5	46.4	7.03128	0.00023	−10255.2	1422960.9	405.0	7.0276	0.0020	[24]	−744.4	4.752	0.011	−282
Xe	54	43+	1500839.2	52.4	6.66294	0.00023	−10985.0	1500870.5	112.6	6.6628	0.0005	This work	−31.3	4.787	0.051	−319
Cs	55	44+	1583686.1	52.4	6.31438	0.00021	−11751.6	1584585.2	502.2	6.3108	0.0020	[24]	−899.0	4.807	0.001	−357
Ba	56	45+	1670951.8	55.8	5.98461	0.00020	−12556.5	1670899.6	139.6	5.9848	0.0005	This work	52.1	4.840	0.001	−401
La	57	46+	1762872.6	59.2	5.67256	0.00019	−13400.8							4.855	0.001	−450
Ce	58	47+	1859670.2	62.9	5.37730	0.00018	−14286.3							4.877	0.001	−504
Pr	59	48+	1961594.5	66.8	5.09789	0.00017	−15212.4							4.893	0.001	−564
Nd	60	49+	2068878.0	70.9	4.83354	0.00017	−16183.0							4.915	0.001	−631
Pm	61	50+	2181773.8	84.7	4.58343	0.00018	−17198.7							4.962	0.050	−711
Sm	62	51+	2300535.2	97.0	4.34681	0.00018	−18260.8	2299379.2	528.7	4.3490	0.0010	This work	1156.1	5.031	0.063	−801
Eu	63	52+	2425518.1	97.5	4.12283	0.00017	−19371.0							5.041	0.050	−892
Gd	64	53+	2556938.6	105.0	3.91093	0.00016	−20530.4	2556825.4	588.4	3.9111	0.0009	[14], This work	113.2	5.089	0.050	−1000
Tb	65	54+	2695156.3	112.0	3.71036	0.00015	−21741.1							5.099	0.050	−1113
Dy	66	55+	2840491.0	149.0	3.52052	0.00018	−23003.9	2840909.1	807.1	3.5200	0.0010	This work	−418.1	5.083	0.081	−1236
Ho	67	56+	2993054.6	152.0	3.34107	0.00017	−24321.0							5.210	0.071	−1397
Er	68	57+	3153660.9	167.0	3.17092	0.00017	−25696.8	3153579.3	994.5	3.1710	0.0010	This work	81.6	5.123	0.074	−1532
Tm	69	58+	3322141.3	151.0	3.01011	0.00014	−27126.7							5.192	0.050	−1714
Yb	70	59+	3498979.8	165.0	2.85798	0.00013	−28614.1							5.317	0.051	−1932
Lu	71	60+	3685038.6	175.0	2.71368	0.00013	−30168.5							5.246	0.050	−2123
Hf	72	61+	3880149.8	190.0	2.57722	0.00013	−31785.8	3880631.8	2409.5	2.5769	0.0016	[1]	−482.0	5.290	0.050	−2367
Ta	73	62+	4085007.5	205.0	2.44798	0.00012	−33473.9	4082299.2	2999.7	2.4496	0.0018	[1]	2708.3	5.299	0.050	−2626
W	74	63+	4299834.6	249.0	2.32567	0.00013	−35225.7	4300705.3	924.8	2.3252	0.0005	[1], [30]	−870.7	5.359	0.061	−2933
Re	75	64+	4525446.9	241.0	2.20973	0.00012	−37046.9							5.351	0.050	−3243
Os	76	65+	4761991.2	261.0	2.09996	0.00012	−38940.5							5.376	0.050	−3602
Ir	77	66+	5010069.0	284.0	1.99598	0.00011	−40911.8							5.401	0.050	−4000
Pt	78	67+	5270247.0	309.0	1.89744	0.00011	−42961.4	5270349.0	434.0	1.8974	0.0002	[27]	−102.0	5.418	0.050	−4437
Au	79	68+	5543006.2	208.0	1.80408	0.00007	−45091.7	5535259.6	6740.6	1.8066	0.0022	[1]	7746.5	5.437	0.011	−4911
Hg	80	69+	5828855.5	213.0	1.71560	0.00006	−47305.3							5.467	0.006	−5475
Tl	81	70+	6128532.9	221.0	1.63171	0.00006	−49605.3							5.483	0.001	−6044
Pb	82	71+	6442541.5	233.0	1.55218	0.00006	−51991.1	6442053.7	1245.0	1.5523	0.0003	[28,29]	487.7	5.505	0.001	−6703
Bi	83	72+	6771518.7	249.0	1.47677	0.00005	−54471.8							5.531	0.005	−7439
Po	84	73+	7116309.4	523.0	1.40522	0.00010	−57048.9							5.539	0.050	−8257
At	85	74+	7477220.7	574.0	1.33740	0.00010	−59723.4							5.578	0.050	−9172
Rn	86	75+	7855047.5	631.0	1.27307	0.00010	−62499.2							5.632	0.050	−10199
Fr	87	76+	8251231.4	692.0	1.21194	0.00010	−65377.7							5.640	0.050	−11293
Ra	88	77+	8665958.4	761.0	1.15394	0.00010	−68363.7							5.663	0.050	−12522
Ac	89	78+	9100383.8	835.0	1.09885	0.00010	−71466.2							5.670	0.050	−13864
Th	90	79+	9553407.5	367.0	1.04675	0.00004	−74678.7							5.802	0.004	−15479
Pa	91	80+	10031340.8	1010.0	0.99688	0.00010	−78019.3							5.700	0.050	−17024
U	92	81+	10527110.2	407.00	0.94993	0.00004	−81471.4	10526482.0	166.2	0.949985	0.00002	[26]	628.2	5.860	0.002	−19040

Similarly, the uncertainty on the DHF contribution, tabulated as $6804 \times 0.005 \times 1.1 = 37$ cm^{-1} (see Table III), becomes $6804 \times 0.025 \times 1.1 = 187$ cm^{-1}. (The factor of 1.1 gives the 10% increase mentioned above to cover the possible model dependence of the assumed nuclear Fermi distribution.) Since we add theoretical uncertainty components in quadrature, the original nuclear size uncertainty (37 cm^{-1}) must first be subtracted from the total (199 cm^{-1}) underneath the square root sign before adding the revised nuclear size uncertainty (187 cm^{-1}) in order to obtain the total revised uncertainty on the transition energy: $\sqrt{199^2 - 37^2 + 187^2} = 271$ cm^{-1}.

The RMBPT values have been obtained as in Ref. [22]. We have reduced slightly the theoretical error in the second- and third-order Coulomb energies, respectively, CC(2) and CCC(3), and the second-order Breit-Coulomb energy BC(2), through the use of larger basis sets. Two small new terms were also added: The second-order Breit term $B^{(2)}_{\mathrm{RPA}}$ in Ref. [22] was generalized to allow terms nonlinear in the Breit interaction

TABLE III. Contributions (cm^{-1}) to the total calculated wave numbers σ and their estimated uncertainties for Bi ($Z = 83$). Values between the dotted lines are from the QED terms.

	$\sigma(D_1)$	Unc.	$\sigma(D_2)$	Unc.
Dirac Hartree Fock	1 559 528	37	6 836 929	41
B(1)	52 830	0	−1481	0
B(rpa)	−1238	0	−299	0
BB(rpa)	−127	0	15	0
Ret(1)	499	0	−8402	0
Ret(rpa)	53	0	−70	0
Other retardation	0	107	0	209
CC(2)	−2616	2	−354	1
BC(2)	−544	1	−265	0
CCC(3)	16	0	−7	0
Nuclear recoil	−68	25	−76	28
SE(val)	−73 091	3	−71 432	3
Uehling (val)	15009	0	17 318	0
WK (val)	−657	62	−781	50
SE (val-exch)	983	14	1029	14
VP (val-exch)	−192	0	−200	0
SE (core rlx)	−1697	23	−814	11
VP (core rlx)	334	0	186	0
Other vertex	0	110	0	73
Two-loop Lamb (val)	238	96	222	90
Total	1 549 261	199	6 771 519	249

[now called BB(rpa) in Table III], and the retardation terms associated with $B^{(2)}_{\mathrm{RPA}}$ were also included [Ret(rpa) in Table III]. However, these two terms are very small, less than the final theoretical uncertainty in all cases. Some remaining retardation effects that arise in second order have not been explicitly calculated ("other retardation"); these arise from two-photon box and crossed-box diagrams (see the Appendix for further details). We have included an uncertainty estimate on the "other retardation" contribution to account for the likely size of these terms. The nuclear recoil contribution is that tabulated in Ref. [22], with an assumed fractional error estimate of $(Z_s\alpha)^2$ to account for omitted higher-order relativistic corrections. The uncertainty in the nuclear recoil term is found to be <17% of the total uncertainty in the calculated D_1 or D_2 transition energies (reaching a maximum in the range Z = 50–60 and falling to <5% at the lowest and highest values of Z reported here).

The QED terms, including the screening effect of the core electrons, were calculated as described in Ref. [3] but using larger basis sets (giving, however, almost no change in the final value for those Z values considered in Ref. [3]). An estimate of the two-loop QED effect has been added by scaling the values for the 1s state of hydrogenic ions given in Ref. [15] according to the normalization of the valence wave function at the origin.

VI. DISCUSSION

Comparison of the experimental and theoretical wavelengths is shown in Figs. 2(a) and 2(b) and tabulated in Tables II(a) and II(b). With the exception of Xe, discussed

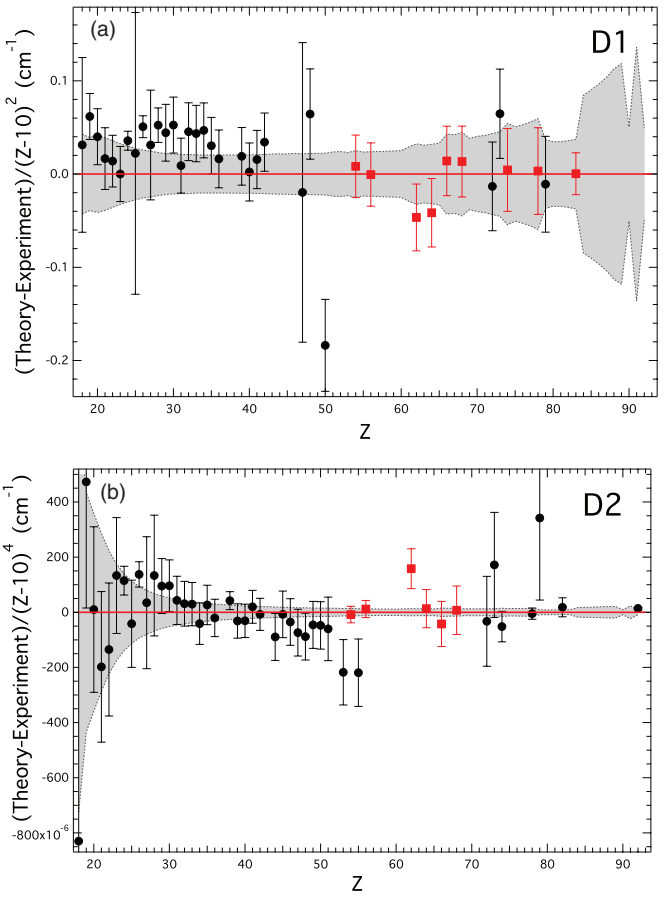

FIG. 2. (Color online) (a) Deviation of the D_1 line from present calculations [$\Delta\sigma$(th-expt.) from Table II], normalized to the second power of the screened nuclear charge. Red squares are the present results. Dotted lines bounding the shaded region are estimated uncertainties in the predictions (irregularities reflect variations in the uncertainties of the nuclear size). (b) As in (a), but for the D_2 line and normalized to the fourth power of the screened nuclear charge. For Gd ($Z = 64$) we show the weighted average of our result from Table I with that of Seely *et al.* [14].

below, the previous experimental values are those tabulated by Reader *et al.* [23], supplemented by several more recent values at high Z [1,11,14,24–30]. Where more than one experimental value is cited in our Table II, the result given is the weighted average. The estimated uncertainty of the calculations is improved over our previous work.

In the case of the Xe D_2 line, Fig. 2(b) and Table II(b) use only our current measurement, which has an uncertainty one fourth the lowest previous reported uncertainty [12] and agrees well with theory, in contrast to three previous measurements [7,12,25] which all agreed with each other but disagreed with theory. In a previous publication [13], we presented evidence for a systematic error due to a line blend at the relatively low collision energies for which the previous experiments were carried out.

A. QED shifts

We quantify the fractional test of QED by the dimensionless parameter $R_{\mathrm{QED}} = \delta/\mathrm{QED}$, where δ is the quadrature sum of the uncertainty in theory and experiment and QED corresponds

TABLE IV. Precise tests of QED for highly charged, few-electron ions. The last column is the figure of merit for testing QED described in the text (smaller values of R represent more stringent tests). The column labeled Δ/δ lists the difference between experiment and theory in units of the quadrature sum of the uncertainty in theory and experiment.

						Theory			Experiment					
	Z	Stage	Seq.	Transition	Name	Energy (eV)	Unc. (eV)	Reference	Energy (eV)	Unc. (eV)	Reference	Δ/δ	QED (eV)	R(%)
U	92	91+	H	$1s$-$2p$	Ly-α	102180.3	0.4	[17] [a]	102178.1	4.8	[33]	0.5	450	1.1
Ar	18	16+	He	$1s^2\ ^1S_0$-$1s2p\ ^1P_1$	w	3139.582	0.005	[32]	3139.581	0.005	[34]	0.2	1.04	0.5
U	92	89+	Li	$2s_{1/2}$-$2p_{1/2}$	D_1	280.650	0.080	[35]	280.645	0.015	[31]	0.1	41.5	0.2
Bi	83	72+	Na	$3s_{1/2}$-$3p_{1/2}$	D_1	192.084	0.024	This work	192.084	0.015	This work	0.0	7.32	0.4

[a]Uncertainty from Ref. [36].

to self-energy and vacuum-polarization terms but does not include the RMBPT correlation contributions described in Sec. V. While this division is at some level arbitrary (both types of contribution include relativistic and field-theoretic effects), it has the merit of permitting some comparison with QED terms in H-like ions, where correlation is absent. For $Z = 83$ (Bi) our result for the D_1 line provides a more precise (smaller R) high-Z test of QED than previously available for Na-like ions [13], and is within a factor of 2 of the most precise test of QED for any highly charged ion [31].

In Table IV, we compare our result to some of the most accurate tests available in other few-electron highly charged ions [17,31–36]. The results for H-like ions were reported by Gumberidze *et al.* [33] in terms of binding energies, but we have used the information contained in their paper to extract the transition energies shown here (this also removes their assumption that there is zero error in the upper calculated level). For high Z, $R_{\rm QED}$ is currently limited by experiment for the hydrogen sequence, by theory for the lithium sequence, and shared roughly equally by theory and experiment for the sodium sequence. For the helium sequence, a recent analysis [37] suggests that the uncertainty in theory and/or experiment may have been underestimated, but in Table IV we quote the results for He-like Ar as originally published [32,34].

While our 78 parts-per-million (ppm) wavelength measurement for Na-like Bi is somewhat less accurate than the 47 ppm measurement for H-like U, our result provides a more precise fractional test of QED, because the magnitude of the transition energy is over 500 times smaller, while the QED contribution is only 60 times smaller. If the theoretical prediction for Na-like Bi were to be improved to the point that its uncertainty did not limit the comparison, our data would test QED to 0.2%, equal to that of Beiersdorfer *et al.* for Li-like uranium [31]. Measurements for the lithium and sodium sequences, however, unlike some measurements for the helium and hydrogen sequences, are typically not absolute (not traced to the meter).

The calculations presented here also increase the precision to which QED can be tested using previously published experimental data because of the reduced theoretical uncertainty (or in some cases, by providing an *ab initio* calculation with which to compare experiments). For example, the D_2 line measured in Na-like uranium by Beiersdorfer *et al.* [26] can now be interpreted as a 0.5% test of QED, somewhat improved over the 0.7% test given by Chen *et al.* [38]. Unfortunately the difference from theory originally reported for that experiment [26] now increases from 0.1 to 1.4 combined standard uncertainties (0.75% of the QED contribution). We note that the reported result from that previous experiment [26] was actually the weighted average of several measurements done with different crystals. Our calculation agrees very well (within 0.02 eV) with the most accurate of the two measurements that were done with a cesium hydrophthalate (CsAP) crystal. That measurement was calibrated with four known lines, which allowed an assessment of calibration nonlinearities, but was assigned a relatively large overall uncertainty to allow for a possible line blend with transitions from other charge states. Two other measurements with an ammonium dihydrogen phosphate (ADP) crystal allowed the line blend to be resolved, but at the expense of a much narrower spectral range, which then limited the wavelength scale to a linear extrapolation of only two calibration lines. The calculations presented here suggest that the result from the lower-resolution measurement may have in fact been more accurate. Additional theoretical and/or experimental work would help resolve this potential issue at the high-Z end of the isoelectronic sequence.

QED is represented by an asymptotic series, so the associated predictions should converge to the correct answer only up to a certain order, and then diverge beyond that [39,40]. In the absence of external electric fields, QED has been calculated up to tenth order (five powers of the fine-structure constant) [41], and experimental accuracy for the anomalous magnetic moment of a free electron [42] gives sensitivity to terms up to four powers of the fine-structure constant. In the presence of the strong electric fields near the nucleus of atoms, the quantum vacuum becomes greatly perturbed and the relative magnitudes of the various QED terms that contribute to the binding of electrons are altered, thus making experiments on free and bound electrons complementary fields of study.

For the electric fields found in neutral hydrogen, QED has been tested up to terms with two virtual photons (two-loop terms), $(\alpha/\pi)^2$ [43,44]. Higher-order terms are included in the theory, but sensitivity to them in experiments is masked by larger uncertainties in the theory of the two-loop terms. In contrast, the present calculation accounts for all two-photon terms (with approximations) to an accuracy that is estimated to be smaller than the magnitude of the three-virtual-photon term CCC(3) for D_1 at $Z < 35$ (at least down to the lowest value of Z calculated here), except in the range $Z = 22$–24, in which it

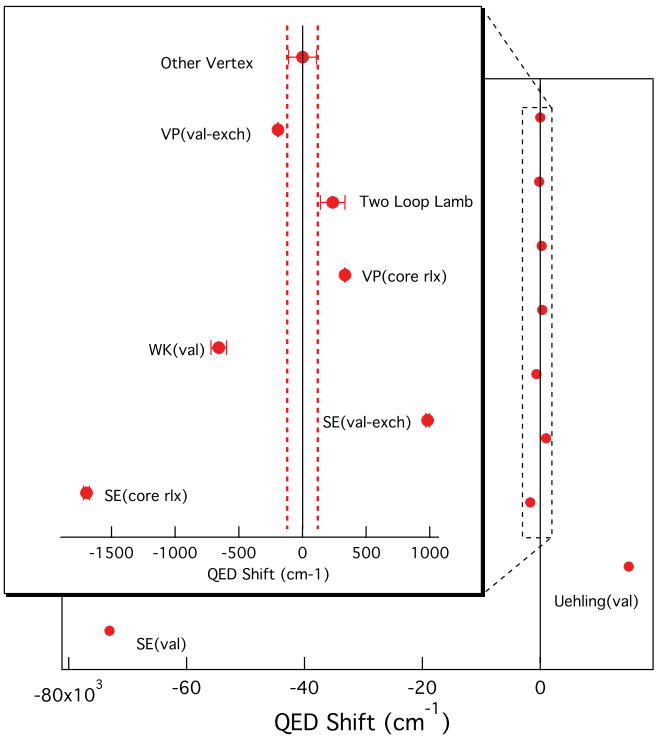

FIG. 3. (Color online) Magnitudes of the QED shifts for the Bi D_1 line, given in Table III. The distance of the points from the vertical line gives the magnitude of the discrepancy with experiment that would result if that point were not included in the sum of all calculated shifts. Dotted lines show the magnitude of the experimental uncertainty.

crosses zero. Although this three-photon term is of correlation type and is not traditionally considered to be part of the QED correction, it represents interesting physics and new experiments with sufficient accuracy to test it would be welcome.

It has been reported earlier [45] that atomic spectroscopy in highly charged Li-like ions can test QED competitively to the most accurate spectroscopy in neutral hydrogen, even though the latter involves at least 14 digits of accuracy [46] (recently increased to 15 digits of accuracy [44]), while the former only involves five digits of accuracy [26]. This is because the two-loop Lamb shift terms [47] are at the forefront of recent investigations, and highly charged ions are particularly sensitive to these terms. Figure 3 shows the magnitude of the two-loop Lamb shift in the Na-like Bi D_1 line, along with the values of the other QED terms listed in Table III. While there appear to be roughly as many positive as negative contributions, the sign of each term is difficult to predict in advance of an explicit full-scale calculation. The largest two terms are the one-photon effects and the rest (shown in the magnified region of the figure) are two-photon effects, except for the WK terms, which are order $(\alpha Z)^2$ corrections to the one-photon vacuum polarization. On this scale, the discrepancy between theory and experiment is virtually zero, so neglecting any one term would result in a discrepancy with experiment equal to the displacement of the point from zero (the dotted red lines indicate the uncertainty in experiment). Points without visible error bars have essentially zero uncertainty.

Although we have just enough accuracy in our measurements to be sensitive to the two-loop Lamb shift, there are uncertainties in both this and other terms in the calculation that are of a similar magnitude. Future work to reduce the theoretical uncertainty in these terms can help improve the possibility of testing these terms individually. A less than a factor of 2 reduction in the uncertainty of theory and experiment would make the results presented here competitive with the two-loop Lamb shift measurement in Li-like U [31], which is reported to be the most precise test of QED in any highly charged ion and competitive with the results obtained in neutral hydrogen. Substantially more experimental accuracy will be needed to probe the two-loop Lamb shift to high precision and to detect new terms, including the following: (i) higher-order (four-photon and higher) correlation (RMBPT) diagrams, which are expected to be of order $1/Z_s \times \mathrm{CCC}(3)$ or $(1/Z_s^2) \times \mathrm{CC}(2)$, (ii) higher-order (three-photon) screening diagrams to the SE or VP, expected to be of order $1/Z_s \times$ (any of the val-exch or core-rlx terms), or $1/Z_s \times$ (two-loop Lamb shift), and (iii) higher-order relativistic corrections to nuclear recoil, expected to be of order $(Z_s\alpha)^2$ times the nuclear recoil term tabulated.

B. Relativistic retardation shifts

Retardation effects (due to the finite speed of light in transverse photon exchange) play an increasingly important role as Z increases. Semiclassically, the importance of retardation effects can be gauged by noting that the velocity of a $3s$ electron in Bi^{72+} is $\alpha Z_s c/n$ (where n is the principal quantum number), and is therefore nearly 20% of the speed of light. In fact, the uncertainty in retardation effects is one of the largest terms in the overall error budget for all values of Z measured here, and represents a challenge to future theoretical work. Figure 4 shows the fractional retardation shift [sum of the calculated terms Ret(1) and Ret(rpa) divided by the total calculated transition energy, in ppm]. Overlaid on the plot is the fractional experimental accuracy (the uncertainty in the measured transition energy, divided by the total measured transition energy, in ppm). Clearly, the accuracy of the experiment and theory at $Z = 83$ is sufficient to be sensitive to the retardation effects. (Note that by retardation we are referring only to retardation corrections in the correlation or

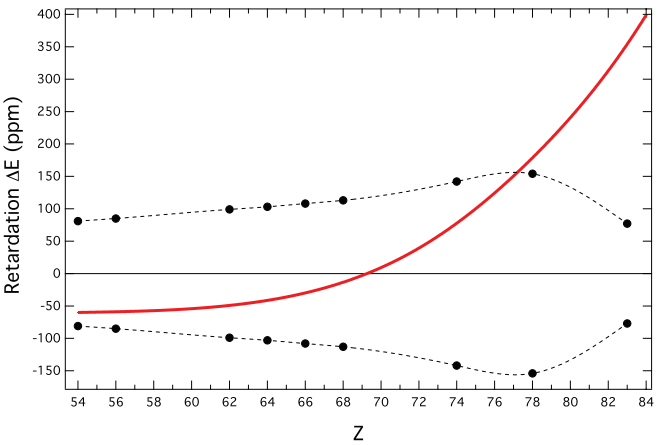

FIG. 4. (Color online) Fractional shift (solid red line) of the D_1 transition energy due to retardation as a function of Z. Black dots show the relative magnitudes of the experimental uncertainties.

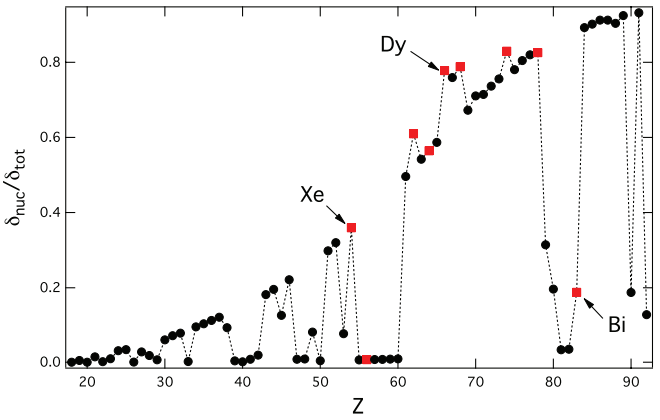

FIG. 5. (Color online) Ratio of uncertainty in transition energy due to assumed nuclear size (Dirac Hartree Fock Unc. from Table III) to the total uncertainty in theory, for D_1 (this ratio is nearly the same for D_2). Ratios for the elements measured here are indicated by red squares.

RMBPT terms. The virtual photon interaction in QED terms is also retarded, and this plays a crucial role in their evaluation.)

C. Nuclear size shifts

The combined accuracy of experiment and theory in the present paper is sufficient to make the results sensitive not only to the nuclear size, but also to the assumed *uncertainty* in nuclear size. Figure 5 shows the magnitude of this sensitivity. The dip near Bi ($Z = 83$) allows the sensitive test of QED presented above.

Our results are also sensitive to variations in the effective nuclear size due to the distribution of isotopes assumed in the sample of ions. For the isotopes of Bi, for example, Angeli and Marinova [48] give a range of nuclear sizes that vary from approximately $r = 5.48$ fm at neutron number $N = 119$ to $r = 5.56$ fm at $N = 130$. Using the nuclear size sensitivity factor given in Table II, the corresponding variation in predicted wave number is over 500 cm^{-1}, compared to our measurement uncertainty of 120 cm^{-1}. Because Bi has a natural abundance that is virtually 100% ^{209}Bi ($N = 126$), however, the isotope size shift is not significant in our measurement. Furthermore, the difference between the nuclear size of ^{209}Bi given by Ref. [48] and our assumed value from Johnson and Soff [17] is one half our assumed uncertainty in nuclear size.

For our measurement of Xe, we injected 90% pure ^{136}Xe. The shift between $N = 136$ and the natural abundance weighted average of $N = 131$ is negligible (<5 cm^{-1}) compared to our present uncertainties, assuming the isotopic variation of nuclear size given by Angeli and Marinova [48].

The other ions used in the present experiment were generated from solid samples of natural isotopic compositions, but reasonable variations in natural isotopic abundance ratios are not expected to significantly alter our overall uncertainty estimates. For high Z, a more detailed estimate of the natural abundance ratios could be used in conjunction with the recent nuclear size results of Angeli and Marinova [48] to reduce our present uncertainty in predicted transition energies.

VII. CONCLUSION

Comparing our data for theory and experiment indicates that QED continues to provide a good description of the electronic structure of highly charged Na-like ions. While the measurements are in good agreement with the new calculations, at the highest values of Z they show a compelling (>3 experimental sigma) deviation from earlier calculations of D_1 by Kim *et al.* [2]. A previous 3-sigma discrepancy in the case of Xe is removed by higher accuracy measurements performed at higher electron collision energies where the ion charge state distribution may be more pure.

At the present level of accuracy, both the finite size of the nucleus and the finite speed of light (retardation effects) must be taken into account. Further work to improve the calculated relativistic retardation effects and determine the higher-order QED vertex corrections would be valuable if higher accuracy experiments become available to more precisely evaluate the overall accuracy of the present predictions. Until then, the present calculations can be taken to represent the preferred values for the D lines of Na-like ions from $Z = 18$ to 92, and, when combined with the present experimental results, provide a precise test of high-Z QED for the sodium isoelectronic sequence.

ACKNOWLEDGMENTS

This work was supported in part by the Office of Fusion Energy Sciences, U.S. Department of Energy. The experiments and data analyzes in this work were performed by J.D.G., D.O., Y.R., and J.R. Collisional-radiative modeling was performed by Y.R. The *ab-initio* calculations were preformed by S.A.B. We thank Glenn Holland for help in installing the elements in the MEVVA.

APPENDIX

In this Appendix, we outline the method used (which follows Ref. [3]) for the theoretical predictions of transition energies in Tables II and III. The transition energy is obtained as the difference of valence removal energies for the two states in the transition. In lowest order, the valence removal energy is given by the valence eigenvalue for a V^{N-1} (Coulomb) Dirac-Hartree-Fock (DHF) potential, that is, the single configuration DHF potential for the closed-shell Ne-like core. Then, following Refs. [16] and [22], the RMBPT terms are constructed from a perturbative expansion about the DHF potential, suppressing negative-energy members of the DHF spectrum and considering only an instantaneous electron-electron interaction given by the sum of the Coulomb and

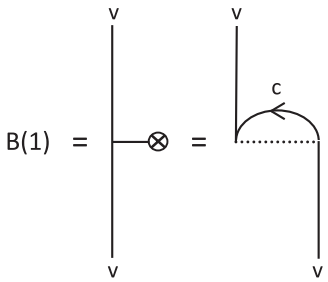

FIG. 6. First-order Breit interaction (dotted line) for a valence state v, involving a sum over the core states c.

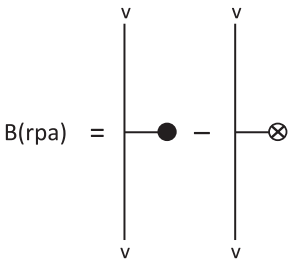

FIG. 7. A second-order Breit correction, B(rpa). The solid blob is the Breit-RPA vertex defined in Fig. 8; the crossed circle is the lowest-order one-body Breit vertex shown in Fig. 6.

Breit interactions. The resulting perturbation expansion can be conveniently represented in terms of Brueckner-Goldstone diagrams analogous to those used in nonrelativistic many-body theory. In first order, only the Breit interaction contributes a term, B(1), shown in Fig. 6.

Various terms enter in second-order RMBPT. The term B(rpa) is shown in Fig. 7; this term involves the random-phase approximation (RPA) vertex for the one-body Breit interaction, the matrix elements of which are obtained from the Dyson-type equation shown in Fig. 8. Iterating this Dyson equation applies second- and higher-order Coulomb screening corrections to the first-order term B(1). We also consider a second-order term BB(rpa) that is nonlinear in the Breit interaction, shown in Fig. 9, which was not considered in the earlier work (but is very small).

Each of the Breit terms discussed above has an associated retardation contribution, which can be obtained by replacing the Breit interaction by the retarded transverse-photon interaction in the Coulomb gauge (see Ref. [16] and references therein). The term Ret(1) corresponds to the change in Fig. 6 when an energy $|\varepsilon_v - \varepsilon_c|$ flows through the transverse-photon propagator, where ε_v and ε_c are DHF eigenvalues for the valence and core states, respectively. (The Breit interaction can be regarded as the zero-frequency limit of the retarded transverse-photon interaction.) A small term Ret(rpa) (not considered previously) arises similarly from Fig. 7; on evaluating the matrix element of the Breit-RPA vertex between valence states v here, the Feynman rules imply that an energy $|\varepsilon_v - \varepsilon_c|$ flows through the transverse photon in the first term on the right-hand side of Fig. 8, while an energy $|\varepsilon_a - \varepsilon_c|$ flows through the transverse

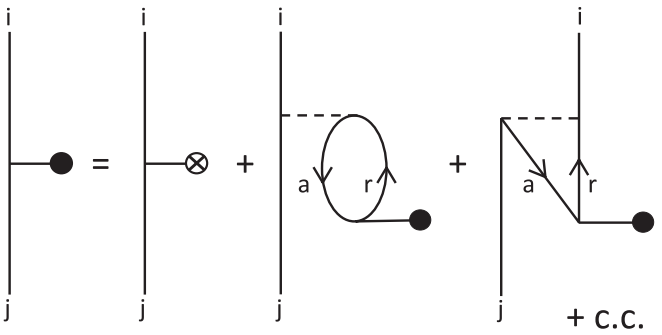

FIG. 8. A Dyson-type equation giving the matrix elements between states i and j of the Breit-RPA vertex. The dashed line is a Coulomb interaction, a are core states, r are excited states, and c.c. denotes the complex-conjugate diagrams of the last two terms on the right-hand side.

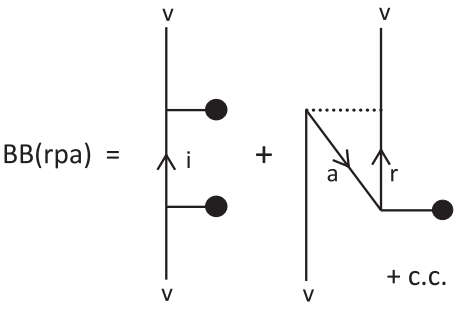

FIG. 9. Second-order nonlinear Breit corrections in RMBPT. The solid blobs are the Breit-RPA vertices (Fig. 8), the dotted line is the Breit interaction, and c.c. denotes the complex conjugate of the second term. The states a are core states, r are excited states, and i includes both core and excited states.

photon (implicit in the RPA blob) in the remaining terms. We also generalize the sum over states r to include negative-energy states (and core states) in these terms, as required in a full QED generalization of these perturbation terms, although this is a much smaller contribution than the retardation effect.

Another second-order term is CC(2), which arises from correlation and is referred to in RMBPT as a two-Coulomb-photon exchange, represented by the Brueckner-Goldstone diagrams in Fig. 10. The Breit-Coulomb term BC(2) is given by replacing the Coulomb interactions in Fig. 10 one at a time with a Breit interaction. It is nontrivial to generalize BC(2) to involve retarded interactions, because the energy flowing through the transverse-photon propagators is not fixed (as it was in the RPA terms above) but varies as part of a loop integral. A full QED generalization of these terms would require evaluation of the box and crossed-box Feynman diagrams shown in Fig. 11, which would bring in a variety of retardation and negative-energy effects. We make an order-of-magnitude estimate of the likely size of the omitted effects ("other retardation") as the larger of the term Ret(rpa) above and a term BB(2) (not tabulated), which we obtain from Fig. 10 by replacing both Coulomb interactions with Breit interactions. The term CCC(3) is analogous to CC(2) but arises from three Coulomb photon diagrams; it can be represented by 12 Brueckner-Goldstone diagrams, as described in Ref. [16], where its evaluation is discussed.

The SE and VP effects cannot be evaluated directly in the DHF potential used for the RMBPT perturbation series, because the order-by-order renormalization procedure requires

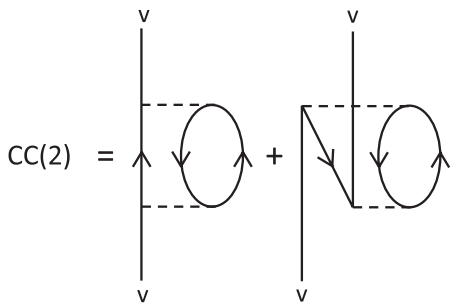

FIG. 10. Brueckner-Goldstone diagrams for second-order two-Coulomb-photon corrections in RMBPT for a valence state v. Exchange variants of each diagram are also included.

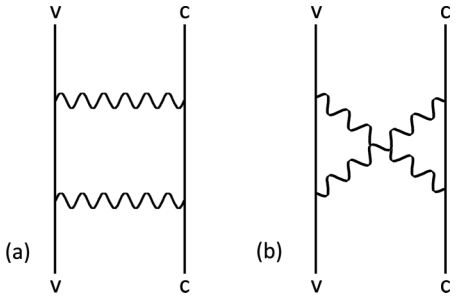

FIG. 11. (a) Box and (b) crossed-box Feynman diagrams. The state v is the valence state, and the diagrams are summed over core states c. Exchange variants of the diagrams also exist, in which v and c at the top of the diagram are interchanged.

a local potential to define the single-particle basis. Following our earlier work [3], we proceed instead as follows. The DHF potential is separated into a sum of the local direct (classical electrostatic) term and the nonlocal exchange term. The former local potential term is used to evaluate the propagators appearing in the valence SE and VP diagrams, shown in Fig. 12, leading to a consistent renormalization of these terms. The exchange part of the DHF potential is then essentially treated in perturbation theory; its screening effect on the valence SE and VP is given to first order by the Feynman diagrams in Fig. 13 (further details can be found in Ref. [3]). Note that these diagrams are in the exchange configuration, in the sense that an ingoing valence (v) line emerges as a core (c) line. The VP terms are decomposed into a dominant Uehling contribution and a smaller Wichmann-Kroll (WK) term; we estimate the latter from hydrogenic values [17] rescaled for the many-electron ion according to the probability density at the origin [3]. A related set of Feynman diagrams, shown in Fig. 14, gives the core-relaxation contribution to the SE or VP, that is, the change in the SE or VP of the core as the valence state changes in the transition. Both sets of Feynman diagrams in Figs. 13 and 14 are technically incomplete; there are also associated vertex-type diagrams that are required to give a gauge-invariant subset of terms [3], examples of which are shown in Fig. 15. For the reasons given in Ref. [3], we assume that these vertex-type terms are numerically small (in the Feynman gauge used to evaluate Figs. 13 and 14), at least in the transition, and omit their evaluation.

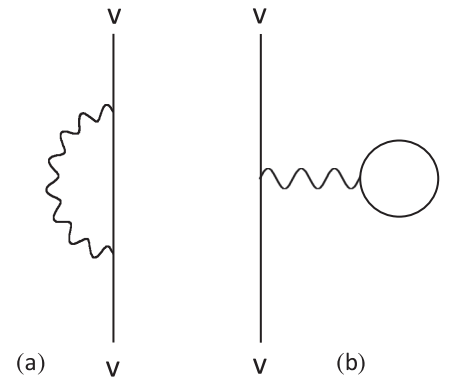

FIG. 12. Feynman diagrams for (a) the valence SE and (b) the valence VP.

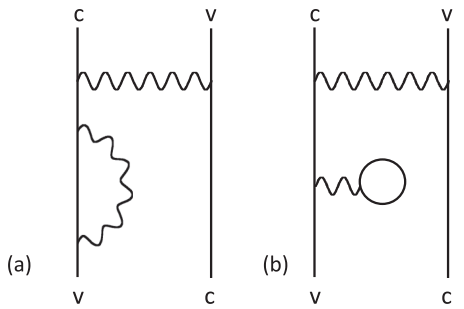

FIG. 13. Feynman diagrams for the valence-exchange ("val-exch") screening corrections to (a) the SE and (b) the VP. The state v is the valence state, and the diagrams are summed over core states c. There are also complex-conjugate diagrams with the SE or VP unit above the exchanged photon.

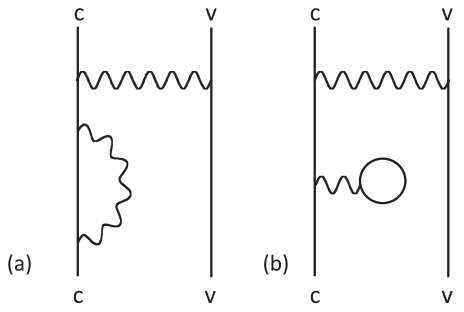

FIG. 14. Feynman diagrams for the core-relaxation ("core rlx") corrections to (a) the SE and (b) the VP. The state v is the valence state, and the diagrams are summed over core states c. There are also complex-conjugate diagrams with the SE or VP unit above the exchanged photon, and exchange variants in which the states v and c at the top of the diagram are interchanged.

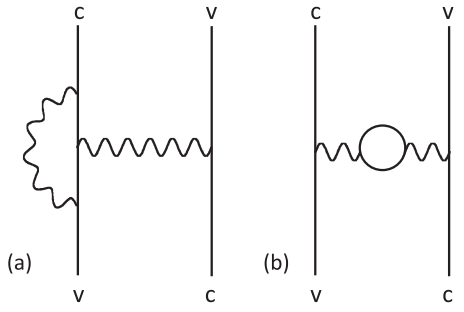

FIG. 15. Vertex-type diagrams omitted from the calculation of the valence-exchange corrections (Fig. 13). Analogous diagrams were also omitted in the calculation of core-relaxation effects (Fig. 14).

[1] J. D. Gillaspy, I. N. Draganić, Yu. Ralchenko, J. Reader, J. N. Tan, J. M. Pomeroy, and S. M. Brewer, Phys. Rev. A **80**, 010501 (2009).
[2] Y. K. Kim, D. H. Baik, P. Indelicato, and J. P. Desclaux, Phys. Rev. A **44**, 148 (1991).
[3] S. A. Blundell, Phys. Rev. A **47**, 1790 (1993).
[4] J. D. Gillaspy, Phys. Scr. T **71**, 99 (1997).
[5] B. Blagojevic *et al*., Rev. Sci. Instrum. **76**, 083102 (2005).
[6] Yu. Ralchenko, I. N. Draganić, D. Osin, J. D. Gillaspy, and J. Reader, Phys. Rev. A **83**, 032517 (2011).
[7] K. Fahy, E. Sokell, G. O'Sullivan, A. Aguilar, J. M. Pomeroy, J. N. Tan, and J. D. Gillaspy, Phys. Rev. A **75**, 032520 (2007).
[8] G. E. Holland, C. N. Boyer, J. F. Seely, J. N. Tan, J. M. Pomeroy, and J. D. Gillaspy, Rev. Sci. Instrum. **76**, 073304 (2005).
[9] J. D. Gillaspy, Phys. Scr. T **65**, 168 (1996).
[10] Yu. Ralchenko, A. Kramida, J. Reader, and the NIST ASD Team, NIST Atomic Spectra Database (version 4.1), http://physics.nist.gov/asd (2011).
[11] J. F. Seely and R. A. Wagner, Phys. Rev. A **41**, 5246 (1990).
[12] E. Trabert, P. Beiersdorfer, J. K. Lepson, and H. Chen, Phys. Rev. A **68**, 042501 (2003).
[13] J. D. Gillaspy, J. Instrum. **5**, C10005 (2010).
[14] J. F. Seely, C. M. Brown, U. Feldman, J. O. Ekberg, C. J. Keane, B. J. MacGowan, D. R. Kania, and W. E. Behring, At. Data Nucl. Data Tables **47**, 1 (1991).
[15] V. A. Yerokhin, P. Indelicato, and V. M. Shabaev, Eur. Phys. J. D **25**, 203 (2003).
[16] W. R. Johnson, S. A. Blundell, and J. Sapirstein, Phys. Rev. A **37**, 2764 (1988).
[17] W. R. Johnson and G. Soff, At. Data Nucl. Data Tables **33**, 405 (1985).
[18] J. D. Zumbro, E. B. Shera, Y. Tanaka, C. E. Bemis, R. A. Naumann, M. V. Hoehn, W. Reuter, and R. M. Steffen, Phys. Rev. Lett. **53**, 1888 (1984).
[19] J. D. Zumbro, R. A. Naumann, M. V. Hoehn, W. Reuter, E. B. Shera, C. E. Bemis, and Y. Tanaka, Phys. Lett. B **167**, 383 (1986).
[20] C. W. De Jager, H. De Vries, and C. De Vries, At. Data Nucl. Data Tables **14**, 479 (1974).
[21] R. Engfer, H. Schneuwly, J. L. Vuilleumier, H. K. Walter, and A. Zehnder, At. Data Nucl. Data Tables **14**, 509 (1974).
[22] W. R. Johnson, S. A. Blundell, and J. Sapirstein, Phys. Rev. A **38**, 2699 (1988).
[23] J. Reader, V. Kaufman, J. Sugar, J. O. Ekberg, U. Feldman, C. M. Brown, J. F. Seely, and W. L. Rowan, J. Opt. Soc. Am. B **4**, 1821 (1987).
[24] J. F. Seely, U. Feldman, C. M. Brown, M. C. Richardson, D. D. Dietrich, and W. E. Behring, J. Opt. Soc. Am. B **5**, 785 (1988).
[25] J. F. Seely, U. Feldman, A. W. Wouters, J. L. Schwob, and S. Suckewer (unpublished; values quoted in [11]).
[26] P. Beiersdorfer, E. Trabert, H. Chen, M. H. Chen, M. J. May, and A. L. Osterheld, Phys. Rev. A **67**, 052103 (2003).
[27] T. E. Cowan, C. L. Bennett, D. D. Dietrich, J. V. Bixler, C. J. Hailey, J. R. Henderson, D. A. Knapp, M. A. Levine, R. E. Marrs, and M. B. Schneider, Phys. Rev. Lett. **66**, 1150 (1991).
[28] P. Beiersdorfer and B. J. Wargelin, Rev. Sci. Instrum. **65**, 13 (1994).
[29] A. Simionovici, D. D. Dietrich, R. Keville, T. Cowan, P. Beiersdorfer, M. H. Chen, and S. A. Blundell, Phys. Rev. A **48**, 3056 (1993).
[30] J. Clementson and P. Beiersdorfer, Phys. Rev. A **81**, 052509 (2010).
[31] P. Beiersdorfer, H. Chen, D. B. Thorn, and E. Trabert, Phys. Rev. Lett. **95**, 233003 (2005).
[32] A. N. Artemyev, V. M. Shabaev, V. A. Yerokhin, G. Plunien, and G. Soff, Phys. Rev. A **71**, 062104 (2005).
[33] A. Gumberidze *et al*., Phys. Rev. Lett. **94**, 223001 (2005).
[34] K. Kubicek, J. Braun, H. Bruhns, J. R. C. Lopez-Urrutia, P. H. Mokler, and J. Ullrich, Rev. Sci. Instrum. **83**, 013102 (2012).
[35] J. Sapirstein and K. T. Cheng, Phys. Rev. A **83**, 012504 (2011).
[36] Y. S. Kozhedub, O. V. Andreev, V. M. Shabaev, I. I. Tupitsyn, C. Brandau, C. Kozhuharov, G. Plunien, and T. Stohlker, Phys. Rev. A **77**, 032501 (2008).
[37] C. T. Chantler *et al*., Phys. Rev. Lett. **109**, 153001 (2012).
[38] M. H. Chen, K. T. Cheng, P. Beiersdorfer, and J. Sapirstein, Phys. Rev. A **68**, 022507 (2003).
[39] F. J. Dyson, Phys. Rev. **85**, 631 (1952).
[40] I. M. Suslov, J. Exp. Theor. Phys. **100**, 1188 (2005).
[41] T. Aoyama, M. Hayakawa, T. Kinoshita, and M. Nio, Phys. Rev. D **85**, 033007 (2012).
[42] D. Hanneke, S. Fogwell, and G. Gabrielse, Phys. Rev. Lett. **100**, 120801 (2008).
[43] P. J. Mohr, B. N. Taylor, and D. B. Newell, Rev. Mod. Phys. **80**, 633 (2008).
[44] C. G. Parthey *et al*., Phys. Rev. Lett. **107**, 203001 (2011).
[45] P. Beiersdorfer, J. Phys. B: At. Mol. Phys. **43**, 074032 (2010).
[46] M. Fischer *et al*., Phys. Rev. Lett. **92**, 230802 (2004).
[47] V. A. Yerokhin, P. Indelicato, and V. M. Shabaev, Phys. Rev. Lett. **91**, 073001 (2003).
[48] I. Angeli and K. P. Marinova, At. Data Nucl. Data Tables **99**, 69 (2013).